Microfluidics based on ZnO/nanocrystalline diamond surface acoustic wave devices

Y. Q. Fu,[1,a] L. Garcia-Gancedo,[2] H. F. Pang,[1,3] S. Porro,[4] Y. W. Gu,[1] J. K. Luo,[5] X. T. Zu,[3] F. Placido,[1] J. I. B. Wilson,[4] A. J. Flewitt,[2] and W. I. Milne[2]

[1]*Thin Film Centre, Scottish Universities Physics Alliance (SUPA), University of West of Scotland, Paisley PA1 2BE, United Kingdom*
[2]*Electrical Engineering Division, Department of Engineering, University of Cambridge, Cambridge CB3 0FA, United Kingdom*
[3]*Department of Applied Physics, University of Electronic Science and Technology of China, Chengdu 610054, People's Republic of China*
[4]*School of Engineering and Physical Sciences, Scottish Universities Physics Alliance (SUPA), Heriot-Watt University, Edinburgh EH14 4AS, United Kingdom*
[5]*Institute of Materials Research and Innovation (IMRI), University of Bolton, Bolton BL3 5AB, United Kingdom*

(Received 12 January 2012; accepted 16 March 2012; published online 3 April 2012)

Surface acoustic wave (SAW) devices with 64 μm wavelength were fabricated on a zinc oxide (ZnO) film deposited on top of an ultra-smooth nanocrystalline diamond (UNCD) layer. The smooth surface of the UNCD film allowed the growth of the ZnO film with excellent *c*-axis orientation and low surface roughness, suitable for SAW fabrication, and could restrain the wave from significantly dissipating into the substrate. The frequency response of the fabricated devices was characterized and a Rayleigh mode was observed at ~65.4 MHz. This mode was utilised to demonstrate that the ZnO/UNCD SAW device can be successfully used for microfluidic applications. Streaming, pumping, and jetting using microdroplets of 0.5 and 20 μl were achieved and characterized under different powers applied to the SAW device, focusing more on the jetting behaviors induced by the ZnO SAW.
 [http://dx.doi.org/10.1063/1.3699974]

I. INTRODUCTION

Surface acoustic waves (SAWs) that propagate on the surface of piezoelectric materials have recently received significant interest due to their large number of potential applications, particularly in biosensing and microfluidics (including micro-droplet transportation, mixing, and ejection), which are two major components for lab-on-a-chip systems.[1,2] SAW-based pumps and mixers possess some significant advantages over other technologies, such as simple device structures (with no moving parts), low fabrication cost, tunable frequency response, and ability to manipulate liquids on a flat surface with great precision.[3,4] ZnO is one of the common piezoelectric materials for the fabrication of SAWs,[5,6] and it can be grown on a variety of substrates, including silicon, making these materials promising for integration with electronic circuitry and many other microfluidics and biosensing techniques, particularly for devices aimed for one-time use, low-cost, fully automation, and mass production.[7–9] Improvement in quality of the ZnO thin films and prevention of significant dissipation of acoustic wave energy into the substrate are two challenges for the successful fabrication of ZnO based SAW for microfluidics and lab-on-chip applications.

The velocity of propagation of surface acoustic waves is highly dependent on the acoustic velocity within the piezoelectric thin films, but is also dependent on the substrate supporting

[a]Author to whom correspondence should be addressed. Electronic mail: Richard.fu@uws.ac.uk.

the piezoelectric material. By selecting a substrate with a high acoustic velocity, the surface acoustic wave velocity can be increased leading to higher frequency operating devices.[4] Diamond possesses the highest acoustic velocity of all materials due to its high elastic modulus, and also it has superior mechanical properties which could increase the acoustic velocity of the piezoelectric layer, thus it is an attractive alternative to other substrates for the fabrication of ZnO film based SAWs. Both experiential work and theoretical analysis reveal that the diamond layer with superior mechanical properties could help to restrain the SAW from dissipating into the substrate, thereby partially confining the wave propagation within the piezoelectric layer and increase the wave velocity.[10–12] Recent progress in chemical vapor deposition (CVD) technology of diamond has made it possible to develop ultra-smooth nanocrystalline diamond (UNCD) films, which allows the growth of piezoelectric films directly on top of the smooth UNCD film, without sacrificing the piezoelectric properties of the active thin films. This would significantly improve the high frequency characteristics of SAW devices as well as increase their electromechanical coupling coefficient. Recently, there has been a lot of research work on the deposition of ZnO on smooth nanocrystalline diamond films to fabricate SAW devices because conventional polycrystalline diamond films have poor surface smoothness.[13–16] Most of these research works are focused on characterization of the ZnO/diamond SAW devices or improvement of sensing with high frequency up to GHz range.[17,18] However, for microfluidics, such as liquid mixing or pumping applications, it is not necessary to have very high frequencies of SAWs up to GHz level, which could result in significant heating effects inside the liquid. So far, few reports are available for exploration of stable and highly efficient droplet ejection or jetting using ZnO or ZnO/diamond SAW devices, and it has yet confirmed whether the ZnO based SAW devices with a few microns of thin film could perform as good as, if not better than, those from the bulk material counterparts, such as $LiNbO_3$. The work reported here shows that the ZnO/UNCD SAW devices can be successfully used for efficient microfluidics applications, especially for liquid jetting, with a frequency in the range of tens of MHz.

II. EXPERIMENTAL

A UNCD coating of 1.2 μm thickness was deposited on Si (100) wafers using a hot-filament chemical vapor deposition (HF-CVD) system (sp3 Diamond Technologies Inc., model 650). A horizontal array of tungsten filaments (0.12 mm in diameter) was fixed over the substrate holder area and heated up to $\sim$2000 °C by Joule heating in a vacuum chamber. Methane (CH_4) was used as the carbon source, and CVD reactions were driven by hydrogen gas. The distance between the substrate surface and tungsten filament was kept at 20 mm. Substrates were heated up to 600 °C directly by the tungsten filaments. Further details of the HF-CVD system can be found in a previously published paper.[19]

ZnO films of $\sim$6 μm thickness were sputter-deposited at room temperature and at a rate of $\sim$50 nm·min^{-1} on the diamond film surface using a novel process known as high target utilization sputtering (HiTUS).[20] HiTUS sputtering is based on a remotely generated high density plasma ($\sim 10^{12}$–10^{13} ions·cm^{-3}, compared to a conventional magnetron plasma, $\sim 10^{10}$ ions·cm^{-3}), which is produced in a side chamber linked by an arm to the main vacuum deposition chamber. Argon plasma is generated by an RF electric field (13.56 MHz, 2.5 kW maximum power) and is then launched into the main deposition chamber (where the metal sputtering target and substrate holder are located) via the interaction of the RF field with an electromagnet. The plasma is then steered onto the target by a second electromagnet. With this layout of magnets, the substrate is not in direct contact with the argon plasma, hence the deposition rate is effectively increased by increasing the flux and energy of the sputtering ions without causing unwanted ion bombardment on the sample. As a consequence, material is deposited at high rates with very low stress, low defect density, smooth surface, and excellent crystallographic orientation.[21,22] The cross-sectional morphology of the deposited ZnO/diamond films was characterized using a scanning electron microscopy (SEM). The crystallinity and crystal orientation of the film were investigated using x-ray diffraction (XRD). Raman spectroscopy was used to characterize the UNCD layers.

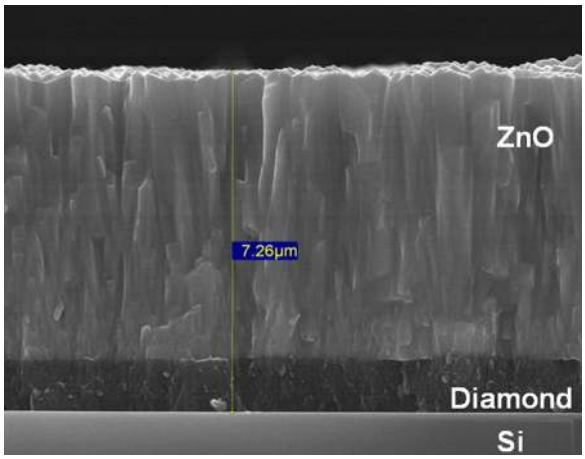

FIG. 1. SEM image showing the columnar structures of the ZnO and UNCD layers on top of Si.

Cr/Au inter-digital transducers (IDTs) of thickness 7/50 nm were fabricated onto the ZnO/diamond layer using a standard photolithography process. The bi-directional IDTs consist of 30 pairs of fingers, with an aperture of 5 mm and a spatial periodicity of 64 μm. Some of the SAW devices were then coated with a CYTOP (Asahi Glass Co.) hydrophobic layer. An HP8752A RF network analyzer was used to measure the resonant frequency and amplitude of the SAW devices. The RF signal from a signal generator was amplified by a power amplifier before being fed into the IDTs, and the RF power applied to the IDTs has been measured using an RF power meter. Water droplets with different sizes were obtained using a micropipette. Droplet movement was measured using a standard video camera from both top and horizontal views.

III. RESULTS AND DISCUSSIONS

A. Film and device characterization

Figure 1 shows cross-section morphology of the ZnO/UNCD film, revealing the columnar morphology for the ZnO and UNCD layers. Both the diamond and ZnO coatings typically grow as long rods along the *c*-axis, which results in apparent columnar grain structures. The refractive index of the ZnO film was measured to be about 2.0, which is near to that of the bulk ZnO, indicating the high quality of the ZnO crystals.

The crystal quality of the films was assessed by XRD analysis. As shown in Fig. 2, the θ–2θ scans of the samples over a broad angle range ($2\theta = 20°$–$80°$) confirm the preferential

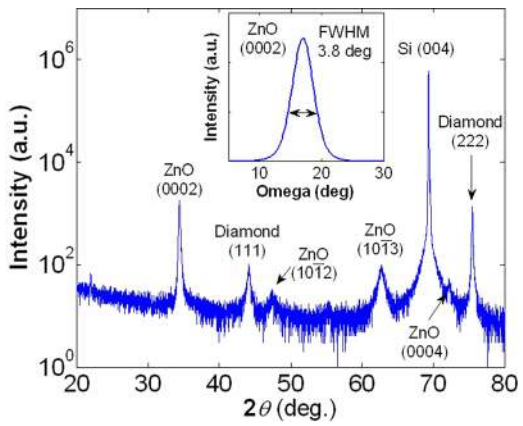

FIG. 2. X-ray diffractogram of ZnO/UNCD films in a θ-2θ configuration. The inset shows the rocking curve of the ZnO (0002) peak.

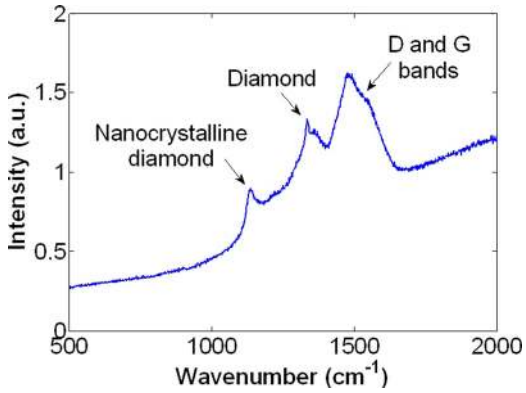

FIG. 3. Raman spectroscopy of UNCD layer. The broad D and G bands are at about 1400 and 1600 cm^{-1}, a sharp diamond peak at 1332 cm^{-1}, and a peak at 1175 cm^{-1} which is the characteristic of nanodiamond particles.

(0002) or *c*-axis growth of the ZnO films. Diffractions of planes corresponding to both the substrate and the diamond layer have also been identified (the identification of the peaks is based on references in Ref. 23). The inset in Fig. 2 presents the rocking curve for the ZnO (0002) diffraction peak, which has a full width at half the maximum (FWHM) of 3.8°, indicating a small angular dispersion of the crystallites around the *c*-axis. This ensures that the ZnO films will have excellent piezoelectric properties. Crystallite sizes were estimated from the values of the Bragg angle and FWHM of the diffraction peak in the 2θ scan using the Debye-Scherrer formula. An average grain size of ~54 nm was found.

Figure 3 shows the Raman spectrum of the UNCD film, which clearly reveals the diamond peak at 1332 cm^{-1} together with the D band (~1370 cm^{-1}) and G band at 1550 cm^{-1} of the disordered carbon structures. The peak observed at ~1170 cm^{-1} is a characteristic of nanodiamond crystals inside the film.

A typical frequency response of the fabricated ZnO/UNCD SAW devices is shown in Fig. 4. The reflection peak (S_{11}) at 65.36 MHz correlates to the fundamental Rayleigh mode wave with a velocity of 4200 m/s. A second peak at 113.75 MHz, corresponding to a wave velocity of 7280 m/s, was also observed. This is a guided Sezawa wave propagating in the interlayer, which occurs when the bulk transverse velocity in the substrate (diamond) is larger than in the top layer (ZnO). A large level of spurious ripples were observed from the Sezawa mode signal, which are mainly due to the triple transit effect, a second order effect where the wave travels three times the distance between input to output source.[24–26] These ripples might also come from the oblique reflection and diffraction effects from the interfaces or different layer boundaries among silicon, diamond, and ZnO.

The ZnO/UNCD SAW device was heated to a temperature up to 150 °C in an environment controlled chamber, and the reflection signals of the Rayleigh peaks were recorded using the

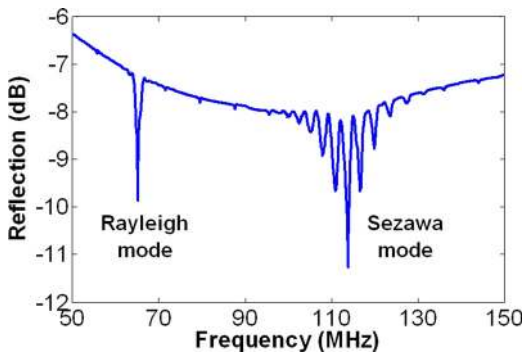

FIG. 4. Typical reflection (S_{11}) measurement of a SAW device with 1.2 μm UNCD layer and 6 μm ZnO layer.

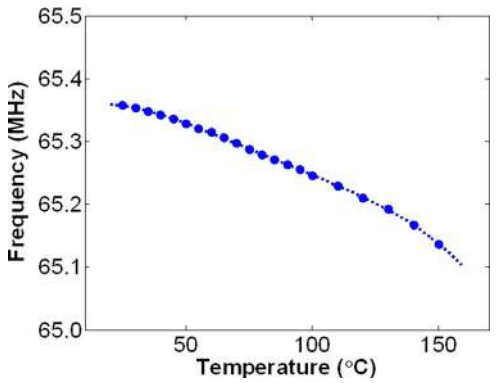

FIG. 5. Frequency shift vs. temperature from 25 °C to 150 °C for ZnO/UNCD device. The dotted line is a guide for the eye.

network analyzer and the results are shown in Fig. 5. The temperature coefficient of frequency (TCF) was calculated using the following equation:[27,28]

$$TCF = -\left(\frac{\Delta f}{\Delta T \times f_0}\right). \tag{1}$$

The TCF value of the ZnO/UNCD SAW device was calculated to be ~26.1 ppm/ °C, comparable to the value of diamond SAW devices of 30 ppm/ °C.[29] This value is much smaller than those reported values of ZnO SAW devices on a silicon substrate (~55–65 ppm/ °C),[6,8] which is mainly attributed to the low TCF value of the diamond layer.

B. Microfluidic evaluation

The as-deposited ZnO film is normally hydrophilic with a typical contact angle of 60–80°. Although the contact angle is reasonable large, the hydrophilic nature of the ZnO surface has the effect of preventing water droplets for moving efficiently on the ZnO SAW device. With a low SAW power of about 50 to 100 mW at a frequency of 65.4 MHz (Rayleigh wave), a typical butterfly streaming pattern within the water droplet can be clearly observed as shown in Fig. 6. By increasing the input SAW power applied to the IDTs on a ZnO film, the water droplet becomes obviously deformed from its original shape (see Fig. 7). The large SAW pressure

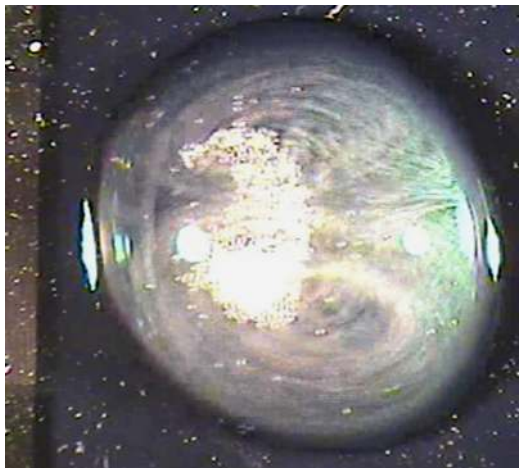

FIG. 6. Internal streaming and mixing inside a 10 μl droplet on a ZnO SAW device. SAW propagates from right to left. Polystyrene particles of 6 μm were added to help mixing visualisation.

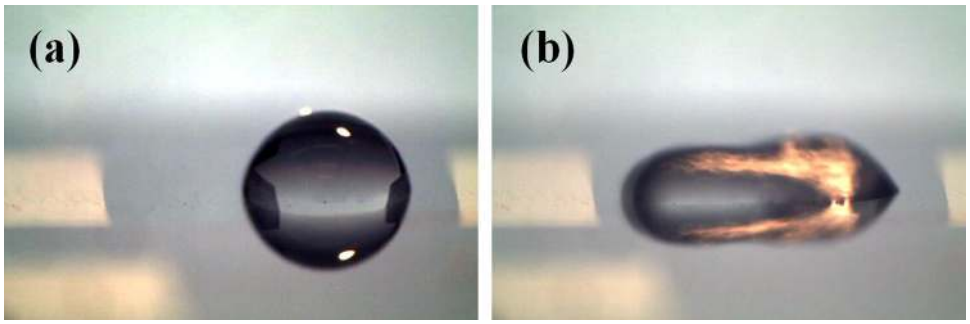

FIG. 7. Liquid droplet flow on untreated ZnO/diamond surface driven by SAW (the SAW propagates from right to the left) (a) original droplet of 10 μl and (b) droplet deformation and spreading on substrate surface with a significant internal streaming at a SAW power of 21 W.

excites and stirs the droplet, causing it to vibrate along with the propagating acoustic wave, and the significant internal streaming inside the droplet can be clearly observed as shown in Fig. 7(b). Finally, the droplet is pushed forward, spreading on the film surface, but due to the hydrophilic nature of the surface, the liquid droplet as a single unit could not be pumped away.

CYTOP coated ZnO/UNCD films show a large contact angle of about 115–120°. In order to compare the sliding force required for the droplet to move on the ZnO film surface, the ZnO film sample with a water droplet on top was tilted to different angles until the droplet began to slide on the film surface (as shown in Figs. 8(a) and 8(b)). At this critical tilting angle, the droplet deforms so that the contact angle on the "trailing edge" of the drop, θ_t, is reduced, whilst that on the leading edge, θ_l, is increased. The driving force, F_s, can be estimated from the asymmetry in these contact angles and the droplet size from:[30,31]

$$F_s = 2R\gamma_{LG}\sin\left(\frac{\theta_t + \theta_l}{2}\right)(\cos\theta_t - \cos\theta_l), \tag{2}$$

where R is the radius of the droplet and γ_{LG} is the liquid-air interfacial energy, (assumed to be 7.2×10^{-2} N/m from Ref. 32). The sliding forces to move the droplet for the untreated and CYTOP coated ZnO/UNCD films were estimated to be 0.13 and 0.026 mN, respectively. Clearly, the surface treatment using the CYTOP increases the contact angle, hence significantly reduces the droplet sliding force, thus enhancing the pumping efficiency.

Pumping and jetting tests using the ZnO/diamond SAW device were performed using water droplets with various SAW powers. Figures 9(a) to 9(c) show examples of pumping movement of a droplet of 2 μl at an RF power of 4 W. The droplet has been deformed dramatically following the Rayleigh angle, and then pushed forward through sliding and rolling, which have been reported in details previously.[5,6,8] Direct observation reveals that with the increase in droplet size, the pumping speed decreases and the droplet moves in a crawling motion because the increase in surface area/volume requires more work to transport the drop.[1–3] The pumping speed increases significantly with the increase of RF power applied to the SAW device.

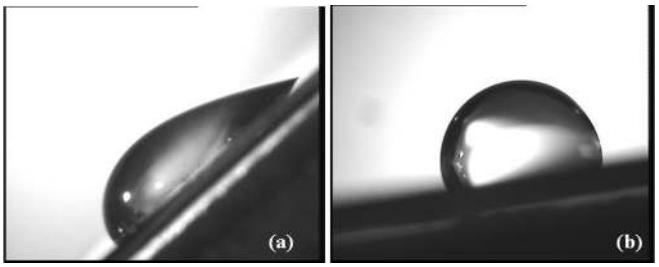

FIG. 8. Starting positions for a 5 μl droplet flow during tilting the substrate of untreated and surface treated ZnO/diamond films on silicon.

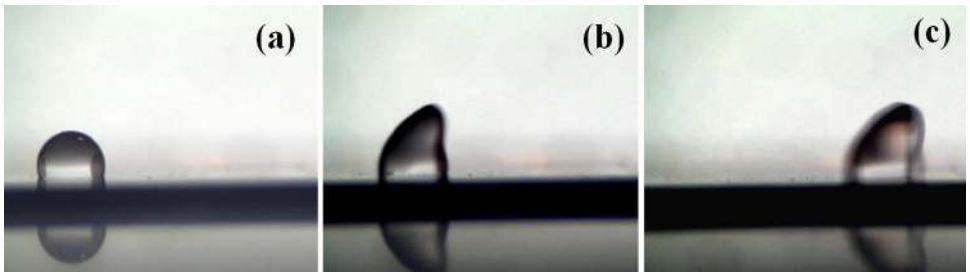

FIG. 9. Droplet pumping for a droplet of 2 μl at an RF power of 4 W at various durations after applying SAW (a) 0 s; (b) 0.08 s; and (c) 0.16 s.

When the input power was increased to a few watts, the water droplet on the film surface began to jump rather than move on the film surface. Figures 10(a) to 10(d) show the jetting behaviors of a water droplet with a size of 15 μl at various SAW powers at a fixed duration of 0.06 s. At a power of 16 W, due to the relatively low SAW energy dissipated into this large droplet, the droplet could only be lifted up to a few millimeters before it dropped down to the device surface (see Fig. 10(a)). With the increase of the SAW powers to 21 W and 26 W, much higher energy is dissipated into the droplet, resulting in generation of stronger jetting effects. Apart from jetting of liquid beam, there are tiny droplets with volume in the range of a few fl to pl are ejected from the base water droplet, forming a mist which have been lifted to much higher positions and ejected further away from the IDT as shown in Figs. 10(b) and 10(c). At an RF power of 32 W, acoustic energy which has been dissipated into the droplet is so high that it causes large inertial pressure in the water droplet to overcome the capillary force,[33] resulting in a coherent cylindrical liquid beam as shown in Fig. 10(d).

The detailed jetting behavior of a water droplet (20 μl) has been recorded at a power of 26 W as shown in Fig. 11. Due to the large droplet size and large contact area on the device substrate, at the initial of jetting, the energy dissipated into the liquid droplet is quite limited in the first 0.02 s, and only partial of droplet has been lifted up (see Fig. 11(b)). The jetting occurs along with the mist formation in the front which has been driven further away as shown in Figs. 11(c) and 11(d). With the increase of duration of the applied SAW power, more energy has been input into the remaining droplet, the droplet was continuously pushed up to a higher

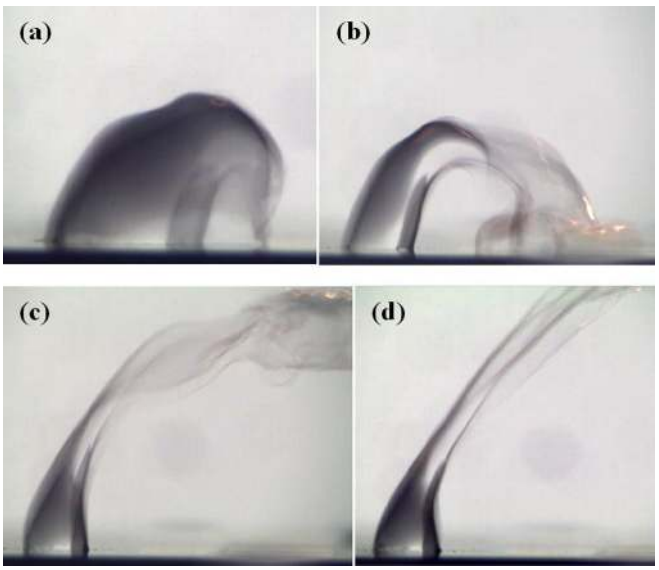

FIG. 10. Ejection of a droplet of 15 μl at different SAW powers at a fixed duration of 0.06 s (SAW propagates from left to right); SAW powers: (a) 16 W; (b) 21 W; (c) 26 W; and (d) 32 W.

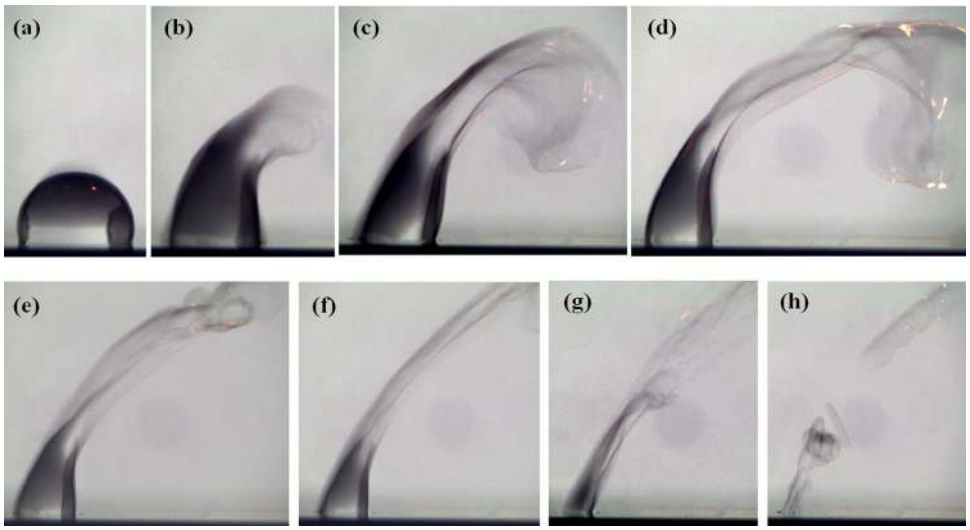

FIG. 11. Droplet ejection a droplet of 20 μl at an SAW power of 26 W (SAW propagates from left to right) (a) original droplet; (b) 0.02 s; (c) 0.04 s; (d) 0.06 s; (e) 0.08 s; (f) 0.1 s; (g) 0.12 s; (h) 0.14 s; (d) 0.16 s; (d) 0.18 s.

position (Fig. 11(e)). A coherent cylindrical liquid jetting beam became dominant after about 0.1 s as shown in Fig. 11(f). The remaining liquid droplet was continuously ejected in such an elongated jetting beam until the entire water droplet has been consumed. Near to the completion of the jetting process, the elongated jet became unstable and consequently broke up into small droplets, and some tiny droplets with sizes in the range from a few pl were ejected from the ZnO SAW surface (see Figs. 11(g) and 11(h)). The whole jetting process for this 20 μm droplet only took about 0.16 s at a SAW power of 26 W. For small water droplets of 5 μl or less, the jetting durations are much shorter, mostly within 0.1 s as listed in Table I. Figure 12 shows the jetting process of a droplet of 2 μl, and the whole droplet has been ejected from surface within 0.06 s. Most liquid droplets have been ejected following the Rayleigh angle. The jetting angle was predicted using Snell's Law and wave propagation velocities of 4200 m/s (ZnO film on diamond) and 1495 m/s (water), $\theta = \sin^{-1}(C_{\text{water}}/C_{\text{ZnO}}) = 20.95°$.[1–3] Our results showed that the measured ejection angle was varied from 13° to 32°, significantly dependent on the water droplet size, RF power, surface hydrophobic treatment, and IDT configuration (including width, shape, and with/without reflectors).

With such a high RF power applied to the ZnO SAW device, it would expect that signficant acoustic heating effect could occur during jetting. The temeprature changes of a droplet of 5 μl at an applied SAW power of 21 W were measured up to a few minutes. The large acoustic energy will cause signficant increase in surface temperature of liquid droplet, up to 80 °C after 3 min. However, results showed that within the first few seconds, the temperature increase is only up to a few degrees. For most of the jetting experiments in this study, the ejection happens within a fraction of a second (generally less than 0.2 s). Within such a short time, the temeprature increase is not significant, thus SAW acoustic heating will not have a significant effect in the jetting process.

TABLE I. Jetting durations as functions of SAW power and droplet size from the ZnO/diamond SAW device.

	Jetting durations at different droplet sizes					
RF power (W)	0.5 μl	2 μl	5 μl	10 μl	15 μl	20 μl
16		0.08 s	0.10 s			
21	0.04 s	0.06 s	0.06 s	0.2 s	0.18 s	
26	0.02 s	0.06 s	0.04 s	0.16 s	0.18 s	0.18 s
32	0.02 s	0.04 s		0.14 s	0.14 s	0.14 s

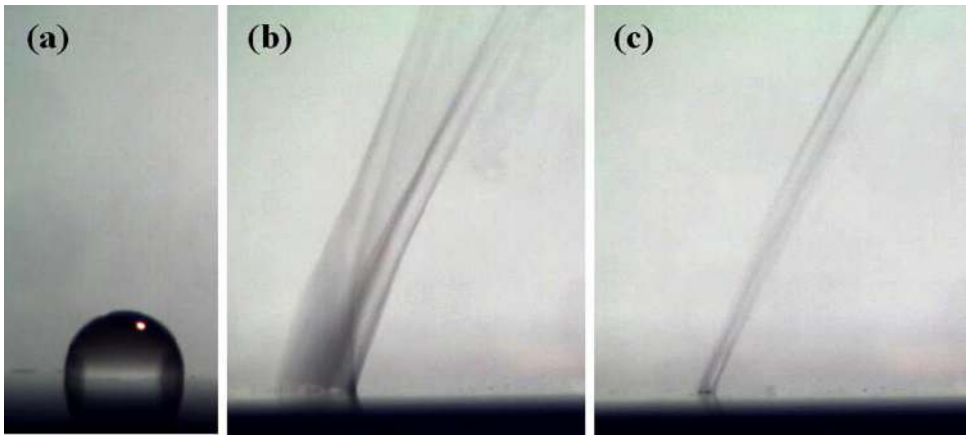

FIG. 12. Droplet ejection a droplet of 2 μl at an SAW power of 21 W (SAW propagate from left to right) (a) original droplet; (b) after 0.02 s; (c) 0.04 s and jetting near to the end.

Figure 13 summarizes the streaming phenomena of the liquid droplets under different powers and different droplet sizes. Clearly for the same water droplet size, there are power boundaries for the various microfluidic phenomena of the liquid droplets, including internal flowing/mixing, pumping, and ejection. Internal flowing and streaming occur at a very low SAW power of a few mW. Higher power will result in the efficient droplet pumping/ejection from SAW surface. For a water droplet with size about 0.5 μl, the ejection is slightly difficult, probably due to the smaller area of the droplet which is not large enough to generate sufficient energy into the liquid droplets for jetting. The jetting was found to become difficult as the water droplet size is more than 10 μl, due to the reduced acoustic energy per width by the droplets as well as the increased mass of the droplet. Both contributions lead to a decreased ejection and streaming in the droplet as the droplet size increases. The streaming velocities (including internal streaming velocity inside droplet, pumping velocity of droplet, and jetting velocity) have been estimated from the analysis of the movie frames for various droplet sizes at different powers, with some of the results shown in Fig. 14. Detailed analysis on the data reveals that there seems a linear relationship between the streaming velocity and square of the RF powers. Guided lines have been drawn to show the differences between different regions of pumping and jetting. However, further experimental work is being done to obtain consolidated and statistical conclusions.

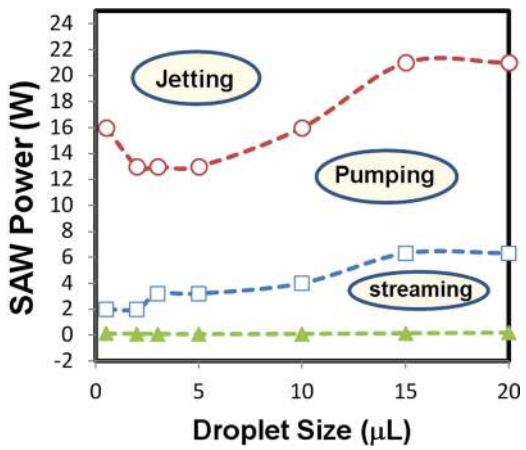

FIG. 13. Summary of streaming phenomena of the liquid droplets under different powers and different droplet sizes (the lines are guided to the eyes only).

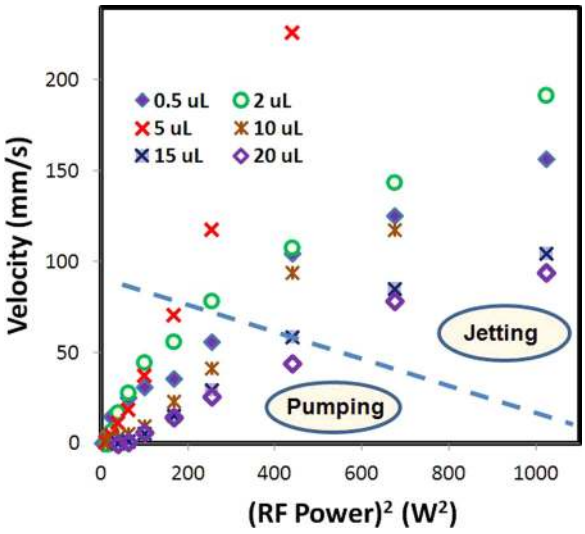

FIG. 14. Estimation of the velocity of streaming, pumping, and ejection as functions of droplet size and RF powers (the line is guided to the eyes only).

IV. CONCLUSIONS

Surface acoustic wave devices with 64 μm wavelength were fabricated on a ZnO/UNCD bi-layer. The relatively smooth surface of the UNCD film, which was deposited using hot-filament CVD, allowed the growth of a ZnO film with excellent *c*-axis orientation and low surface roughness, suitable for SAW fabrication. The frequency response of the fabricated devices was characterized using a network analyzer and a Rayleigh mode was observed at ~65 MHz. This mode was utilised to demonstrate that ZnO/UNCD SAW devices can be successfully used for microfluidic applications. Streaming, pumping, and jetting of microdroplets of different sizes were achieved under different powers applied to the IDTs.

ACKNOWLEDGMENTS

The authors acknowledge support from the Royal Society-Research Grant (RG090609), Carnegie Trust Funding and Royal Society of Edinburgh. L. Garcia-Gancedo, J. K. Luo, A. J. Flewitt, and W. I. Milne acknowledge the financial support of the EPSRC, through Grant Nos. EP/F063865/1 and EP/F06294X/1.

[1]L. Y. Yeo and J. R. Friend, Biomicrofluidics **33**, 012002 (2009).
[2]J. R. Friend and L. Y. Yeo, Rev. Mod. Phys. **83**, 647–704 (2011).
[3]A. Wixforth, J. Assoc. Lab. Autom. **11**(6), 399 (2006).
[4]J. K. Luo, Y. Q. Fu, Y. Li, X. Y. Du, A. J. Flewitt, A. J. Walton, and W. I. Milne, J. Micromech. Microeng. **19**, 054001, (2009).
[5]Y. Q. Fu, J. K. Luo, X. Y. Du, A. J. Flewitt, Y. Li, G. H. Markx, A. J. Walton, and W. I. Milne, Sens. Actuators B **143**, 606–619 (2010).
[6]X. Y. Du, Y. Q. Fu, J. K. Luo, A. J. Flewitt, and W. I. Milne, J. Appl. Phys. **105**, 024508 (2009).
[7]C. Jagadish and S. J. Pearton, *Zinc Oxide Bulk, Thin Films and Nanostructures: Processing, Properties and Applications* (Elsevier Science Ltd., 2006).
[8]X. Y. Du, Y. Q. Fu, S. C. Tan, J. K. Luo *et al.*, Appl. Phys. Lett. **93**, 094195 (2008).
[9]W. L. Dang, Y. Q. Fu, J. K. Luo, A. J. Flewitt, and W. I. Milne, Superlattices Microstruct. **42**, 89 (2007).
[10]V. Mortet, O. A. Williams, and K. Haenen, Phys. Status Solidi A **205**, 1009 (2008).
[11]H. Nakahata, A. Hachigo, K. Higaki, and S. Fujii, IEEE Trans. Ultrason. Ferroelectr. Freq. Control **42**, 362 (1995).
[12]S. Fujii, S. Shikata, T. Uemura, H. Nakahata, and H. Harima, IEEE Trans. Ultrason. Ferroelectr. Freq. Control. **52**, 1817–1822 (2005).
[13]S. Wu, R. Ro, and Z. X. Lin, Appl. Phys. Lett. **94**, 032908 (2009).
[14]S. Fujii, Phys. Status Solidi A **208**(5) 1072–1077 (2011).
[15]B. Bi, W.-S. Huang, J. Asmussen, and B. Golding, Diamond Relat. Mater. **11**, 677–680 (2002).
[16]S. Bensmaine, L. Le Brizoual, O. Elmazria, J. J. Fundenberger, M. Belmahi, and B. Benyoucef, Diamond Relat. Mater. **17**, 1420 (2008).
[17]F. Benedic, M. B. Assouar, F. Mohasseb, O. Elmazria, P. Alnot, and A. Gicquel, Diamond Relat. Mater. **13**, 347 (2004).

[18]O. Elmazria, F. Benedic, M. El Hakiki, H. Moubchir, M. B. Assouar, and F. Silva, Diamond Relat. Mater. **15**, 193 (2006).
[19]S. Porro, G. De Temmerman, D. A. MacLaren, S. Lisgo, D. L. Rudakov, J. Westerhout, M. Wiora, P. John, I. Villalpando, and J. I. B. Wilson, Diamond Relat. Mater. **19**, 818 (2010).
[20]A. J. Flewitt, J. D. Dutson *et al*., Semicond. Sci. Technol. **24**, 085002 (2009).
[21]L. García-Gancedo, J. Pedrós, A. J. Flewitt, W. I. Milne, J. K. Luo, and C. J. B. Ford, "c-axis oriented zinc oxide thin films from high rate room temperature deposition," J. Appl. Phys (submitted).
[22]L. Garcia-Gancedo, J. Pedrós, A. J. Flewitt, W. I. Milne, G. M. Ashley, J. K. Luo, and C. J. B. Ford, in *IEEE Ultrasonics Symposium* (IEEE, 2010), pp. 1064–1067.
[23]International Centre for Diffraction Data (ICDD), ZnO file number 36-1451, Diamond ICDD 06-0675.
[24]C. K. Campbell, *Surface Acoustic Wave Devices for Mobile Wireless Communications* (Academic, New York, NY, 1998).
[25]R. Marcelli, M. Rossi, and P. De Gasperis, J. Appl. Phys. **73**, 3082 (1993).
[26]B. Lewis and R. G. Arnold, IEEE Trans. Sonics Ultrason. **32**, 409 (1985).
[27]Y. Yoshino, M. Takeuchi, K. Inoue, T. Makino, S. Arai, and T. Hata, Vacuum **66**, 467 (2002).
[28]F. Benedic, M. B. Assouar, P. Kirsch, D. Moneger, O. Brinza, O. Elmazria, P. Alnot, and A. Gicquel, Diamond Relat. Mater. **17**, 804 (2008).
[29]H. Nakahata, S. Fujii, K. Higaki, A. Hachigo, H. Kitabayashi, S. Shikata, and N. Fujimori, Semicond. Sci. Technol. **18**, S96 (2003).
[30]D. Beyssen, L. Le Brizoual, O. Emazria, and P. Alnot, in *IEEE Ultrasonics Symposium* (IEEE, 2005), Vol. 2, p. 1028.
[31]C. G. L. Furmidge, J. Colloid Sci. **17**, 309 (1962).
[32]K. Fukagata, N. Kasagi, P. Ua-arayaporn, and T. Himeno, Int. J. Heat Fluid Flow **28**, 72 (2007).
[33]M. K. Tan, J. R. Friend, and L. Y. Yeo, Phys. Rev. Lett. **103**, 024501 (2009).